OPTOACOUSTIC SYSTEMS FOR SUBSURFACE MATERIALS CHARACTERIZATION

Gopi N. Maguluri, Lei Sui, Ronald A. Roy and Todd W. Murray

Department of Aerospace and Mechanical Engineering, Boston University, Boston, MA, 02215

ABSTRACT. Optoacoustic imaging is a promising technique for the detection of subsurface optical inhomogeneities in optically turbid media. A pulsed laser is used to irradiate a sample volume where it is absorbed and causes rapid heating. Ultrasonic waves are launched through the thermoelastic effect and are detected at the sample surface. The detected ultrasonic transients are related to the position dependent absorption coefficient allowing for imaging of the absorbed electromagnetic energy distribution. In this work, the use of optical interferometry for the detection of optoacoustic signals is explored using three detection schemes: a photorefractive crystal based interferometer, a Fabry-Perot sensor head which is coupled directly to the specimen and a Michelson interferometer. Experimental results are presented demonstrating optical detection of optoacoustic transients in both homogeneous, absorbing tissue phantoms and optically turbid tissue phantoms. The measured optoacoustic signal profiles are compared to theoretical predictions and the absorption (homogeneous media) coefficients of the phantoms determined.

INTRODUCTION

Laser based ultrasonic techniques use lasers to generate acoustic waves through the thermoelastic effect, which propagate through the specimen of interest and are subsequently detected using an optical probe [1-3]. Analysis of the acoustic wave propagation (velocity, dispersion, attenuation, etc.) yields information about the physical properties of the specimen. A related materials characterization technique, often referred to as optoacoustic imaging (OAI) or optoacoustic spectroscopy, also uses lasers to excite a material and launch acoustic waves, which are subsequently detected at the specimen surface. However, in optoacoustic imaging the detected *waveform shape* is used to obtain information about the *optical* properties of the specimen and to determine the distribution of absorbed electromagnetic energy in the target material. Optoacoustic tomography has seen widespread use in medical applications including breast cancer imaging, cellular microscopy, depth determination of port wine stain and glucose monitoring in the blood [4,5]. In these applications a short-pulsed laser is used to irradiate tissue where it is selectively absorbed in naturally occurring chromophores. Regions of high optical absorption heat up more than the surrounding tissue giving rise to stronger acoustic signals. In a breast cancer imaging application, for example, light is selectively absorbed in developing tumors due to increased local blood flow in the tumor region. The acoustic signals detected at the tissue surface are processed and back-projected to give a 3-D representation of the absorbed electromagnetic energy distribution within the tissue. Optoacoustic spectroscopy also provides a convenient means to measure the optical absorption and scattering properties of materials.

In this work, the use of optical probes for the detection of optoacoustic transients is explored. Optical detection offers a number of advantages over contact transducer detection in OAI applications. First, OAI requires high bandwidth receivers for high-resolution near-surface imaging applications (early tumor detection, dermatological applications, etc.). Optical detection systems easily cover the useful frequency range for medical imaging. In addition, optical detection systems offer the possibility of developing a truly remote, noncontact optoacoustic imaging system. Finally, OAI can be performed in either backward or forward detection modes corresponding to the receiving transducers on the same side of the sample as the illumination source or opposite side, respectively as illustrated in Fig. 1. Much of the work in the field of OAI has been done in forward mode using either a single element or arrays of PZT, PVDF, or lithium niobate transducers. Forward mode is somewhat easier to implement than backward mode because the source and receivers do not have to be co-located. However, in many potential applications of OAI, forward mode detection is not possible because the backside of the sample is not accessible. Backward mode detection can be difficult to implement using conventional transducers because it requires an optically transparent sensor head, which allows the excitation laser to reach the specimen, while also providing a means of coupling the ultrasound from the specimen to the transducer. Optical detection of acoustic waves provides a solution to this difficulty and can be implemented using a dichroic sensor head, which is transparent at the excitation wavelength and reflective at the detection wavelength.

Various researchers have proposed optical detection for OAI. The systems have been based on acoustically induced change in refractive index [6], polymer film based Fabry-Perot detection of acoustic waves [7] and single point interferometry systems, which are scanned over the specimen [8]. In this work, experimental results are presented for optoacoustic signals detected with several different optical detection schemes. The specific systems that have been used are a) a Fabry-Perot interferometer, similar to the etalon based system described in [9], b) a photorefractive based detection scheme and c) a path stabilized Michelson interferometer. A theoretical formulation is presented for one-dimensional generation of acoustic waves in a two layer media to illustrate the relationship between the absorbed electromagnetic energy distributions and generated acoustic signals.

THEORY

The theory of pulsed laser generation of ultrasound in a wide variety of material systems is well developed [1,10,11]. Here, the one dimensional case of laser generation of ultrasound in a two-layer material system is considered and used to predict the ultrasonic displacements. The measured displacement can then be used to estimate the optical absorption coefficient of the specimen. Referring back to Fig. 1, the top layer of the model is a transparent sensor head. The role of this material in all-optical OAI systems is to provide a smooth surface off of which the detection probe can be reflected. The lower layer represents the specimen of interest. Ultrasound is generated in the specimen and is either detected in forward mode after propagating through the specimen, or in backward mode after coupling to the sensor head. For simplicity, the effects of thermal diffusion are not included in the model. This assumption holds for cases where the thermal diffusion length is small compared to the optical absorption depth such that heat is not able to escape from the irradiated region during the time scale of interest. The sensor head is assumed to be transparent to the generation beam.

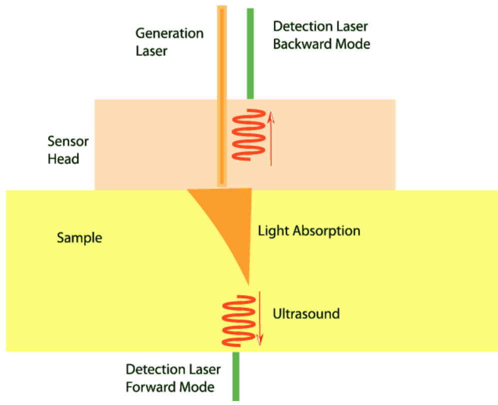

FIGURE 1. Generation of optoacoustic signals, backward and forward mode optical detection

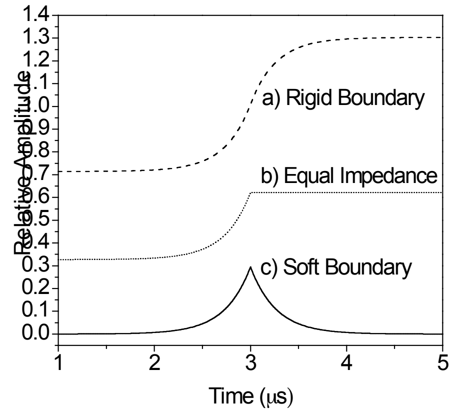

FIGURE 2. Effects of boundary on the forward mode detection plots. Z_1, acoustic impedance of sensor head and Z_2, acoustic impedance of the sample a) $Z_1/ Z_2 >>1$, b) $Z_1/ Z_2 =1$, c) $Z_1/ Z_2 <<1$

Assuming homogeneous absorption in the specimen, the absorbed laser power is given by:

$$I = I_0 f(t)\alpha \exp\left(-\alpha z\right) \tag{1}$$

where I_0 is the incident laser power per unit area, α is the optical absorption coefficient and $f(t)$ is the time dependence of the laser source. Absorbed optical energy from the laser source causes heating in the sample with a subsequent rise in temperature. The temperature distribution in the sample can be obtained by solving the heat conduction equation and is given as follows:

$$\frac{\partial T}{\partial t} - D\frac{\partial^2 T}{\partial z^2} = \left[\frac{\alpha I_o}{\rho C_p}\right]\delta\left(t\right)\exp\left(-\alpha z\right) \tag{2}$$

$$T(z,t) = \left[\frac{\alpha I_o}{\rho C_p}\right]H\left(t\right)\exp\left(-\alpha z\right) \tag{3}$$

where $H\left(t\right)$ is the Heaviside's unit step function, ρ , C_p and D are the density, specific heat at constant pressure and diffusivity of the sample, respectively. $T(z,t)$ is the temperature distribution in the sample, which becomes the source term in the elastic wave equation. We have assumed a delta function time dependence for the laser source, and the interface between the sensor head and specimen is taken at z = 0. Both the sensor head and specimen are taken as semi-infinite. Solutions can be found by solving the elastic wave equations with the boundary conditions of continuity of stress and displacement at the interface.

$$\frac{\partial^2 u_{tr}}{\partial z^2} - \left(\frac{1}{c_{tr}{}^2}\right)\frac{\partial^2 u_{tr}}{\partial t^2} = 0 \tag{4}$$

$$\frac{\partial^2 u}{\partial z^2} - \left(\frac{1}{c^2}\right)\frac{\partial^2 u}{\partial t^2} = \beta\frac{\partial T}{\partial z} \tag{5}$$

with BC: $$\sigma_{tr} = \sigma, \;\; u_{tr} = u \quad at \;\; z = 0 \tag{6}$$

The parameters u, c, ρ and $u_{tr}, c_{tr}, \rho_{tr}$ are the displacement, longitudinal wave speed and density of the sample and the sensor head respectively and β is the thermal coefficient of volume expansion of the sample. Solutions obtained for backward and forward mode using Laplace transform techniques are given by

$$u_{backward} = \frac{\beta I_0 c}{C_p(\rho c + \rho_{tr} c_{tr})}(1 - e^{-\alpha c(t + \frac{z}{c_{tr}})}) H(t + \frac{z}{c_{tr}}) \tag{7}$$

$$u_{forward} = \frac{\beta I_0}{C_p \rho}[-e^{-z\alpha}(1 - \cosh(t\alpha c)) + \frac{H(t - \frac{z}{c})}{(\rho c + \rho_{tr} c_{tr})} \times$$

$$\{\rho_{tr} c_{tr}(1 - \cosh((t - \frac{z}{c})\alpha c)) - \rho c \sinh((t - \frac{z}{c})\alpha c)\}] \tag{8}$$

The forward mode solution is shown in Fig. 2 illustrating the effects of changing the acoustic impedance of the sensor head.

The physical explanation for the signals obtained in Fig. 2 can be given by treating the exponentially attenuating temperature source as discrete planar sources of varying strength. As the material expands, the planar sources generate waves in both positive and negative *z* directions. The magnitude of each wave is proportional to the temperature at its source. Since the temperature decays exponentially, the displacement of the closest source will be small. The next wave to arrive at the observer's location will be from a temperature source that is further from the observer. The magnitude of this displacement wave will be greater than that of the previous wave because the temperature at the source location is greater. As the process continues, the displacement at the observer's location will continue to increase exponentially until the wave generated by the temperature source at the surface arrives at the observer. This is same for all the boundary conditions. In the case of a rigid boundary (acoustic impedance of sensor head $Z \Rightarrow \infty$), the negative displacement waves will change their sign at the boundary (to satisfy the boundary condition) and become positive displacement waves of decreasing amplitude traveling in the positive z direction which will add up to the displacement at the detection. In the case of soft boundary (acoustic impedance of sensor head $Z \Rightarrow 0$), the surface is stress free and the negative displacement waves reflect from the boundary without any change of sign. This causes the exponential rise to fall back to zero, canceling the positive displacements previously caused at the detection spot. In the case of equal impedance, there is no reflection and the displacement remains constant.

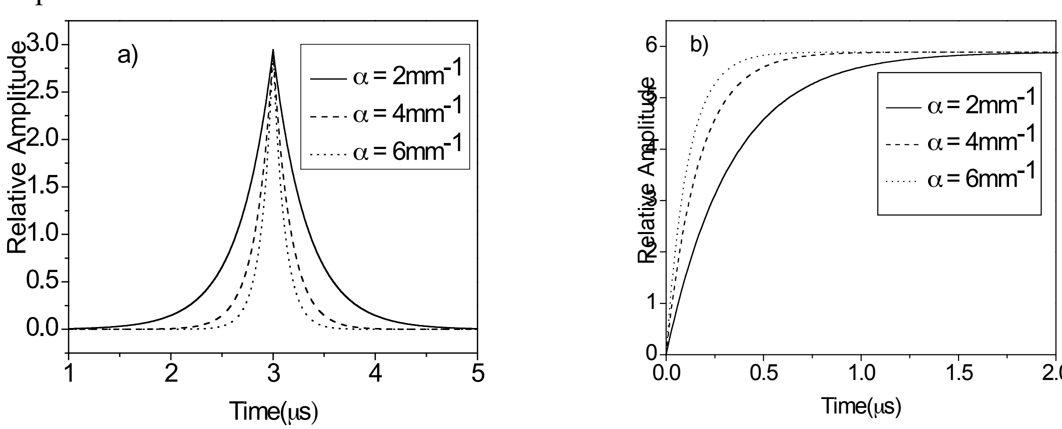

FIGURE 3. Ultrasonic displacements as a function of absorption depths for the soft boundary case a) Forward mode at z=4.5mm and c=1.5mm/μs b) Backward mode at z=0 and c=1.5mm/μs

Fig. 3 shows the effects of varying the optical absorption depth on both the forward and backward mode displacement signals. Fig. 3a shows the ultrasonic displacement signals in forward mode as a function of absorption depth. In this case the detection spot is at a depth of $z = 4.5$mm, and the sound velocity in the sample c = 1.5mm/μs. The ultrasonic signals can be seen to broaden as the absorption depth increases. Fig. 3b shows the plots in backward mode at z =0 for several absorption depths.

EXPERIMENTAL SETUP

Experiments were performed using three different types of interferometry systems: a photorefractive based interferometry system similar to that described in [12,13], a Fabry-Perot based system where the sensor head acts as one of the Fabry-Perot cavity mirrors [9], and a path stabilized Michelson interferometer [14]. These interferometry systems have been described in detail in the literature. Each of these systems has advantages and disadvantages for OAI. Photorefractive based systems, for example, can be used off of optically rough surfaces and can be easily multiplexed to create detection arrays. The Fabry-Perot based sensor head is predicted to have extremely high sensitivity, approaching that of piezoelectric transducers. It was also found that a Michelson interferometer could be used to detect signals directly off of specimen surface in cases where surfaces are optically flat or coated with reflecting media. The generation laser used was a pulsed Nd:YAG laser at 1064nm with energy 50mJ and a pulse width of 7ns. The detection laser used was a continuous wave Nd:YAG laser operating at 532nm with an optical power of 200mW.

Preliminary experiments were performed on homogeneously absorbing neutral density filters with well-characterized optical properties. In addition tissue-mimicking phantoms were fabricated following the procedure stated in [15]. In this recipe, 9.735g of acrylamide and 0.265g of bis-acrylamide (Sigma Chemical) were dissolved in 50ml of deionized water. For mimicking the breast tissue, polystyrene beads of diameter 0.4μm at a density of 0.1spheres/cubicμm were added as scattering particles. The addition of polymerizing initiator of 0.02g of ammonium persulfate and 0.2ml of TEMED (Sigma Chemical) creates a 20% acrylamide gel. The density of the spheres was calculated using Mie theory to achieve a reduced scattering coefficient of approximately 8cm^{-1} at 1064nm. The fabricated scattering phantom molded in a petri dish is shown in Fig. 5.

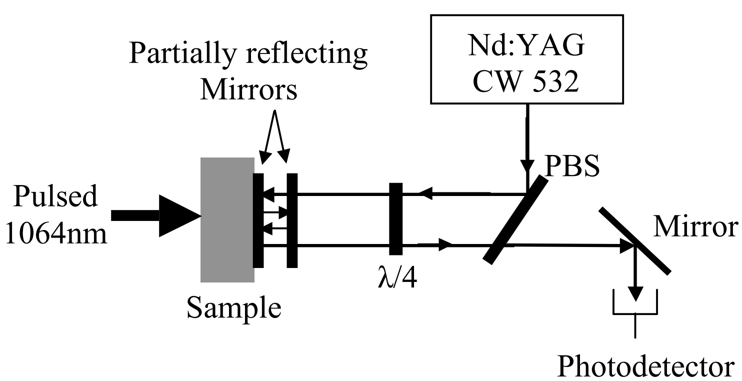

FIGURE 4. Experimental setup for the Fabry-perot interferometer PBS: Polarizing beam splitter, λ/4: Quarter wave plate, CW 532: Continuous wave laser at 532nm

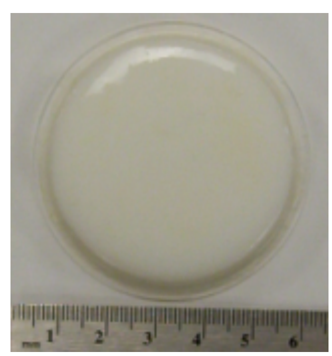

FIGURE 5. Scattering phantom with polystyrene beads

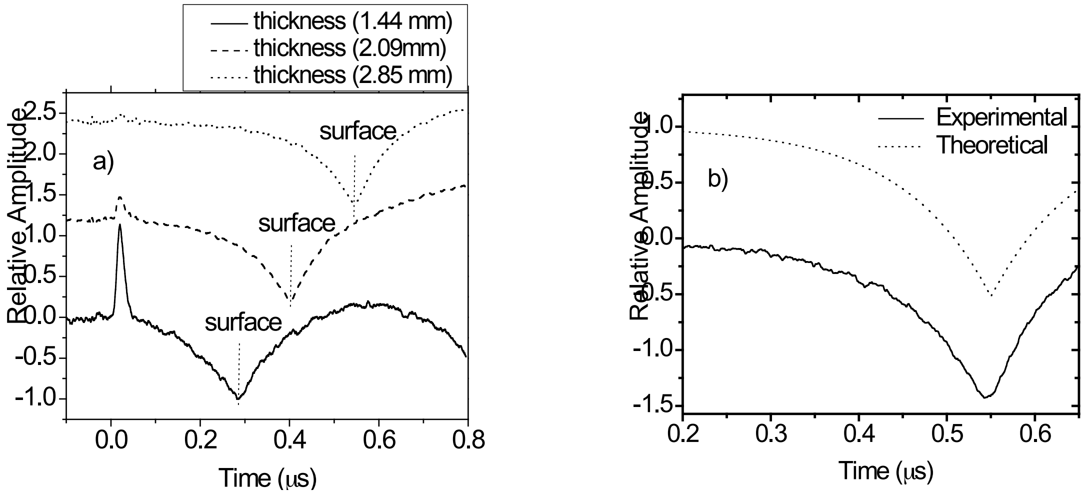

FIGURE 6. a) Forward mode detection plots of a homogeneously absorbing neutral density filters at different thickness and b) comparison of theory and experiment for the filter of thickness 2.85mm

EXPERIMENTAL RESULTS

Measurements of optoacoustic signals detected on homogeneous neutral density filters using the photo-refractive based interferometry system are given in Fig. 6a. It was found that all 3 filters had same absorption coefficient but cut to different thickness to achieve desired absorption characteristics. The velocity of the ultrasonic wave in the filter is 5.81mm/μs. The initial spike at around time $t=0$ is due to the generation beam leaking into the photodetector. Comparison of the theoretical waveform calculated from the absorption coefficient of 1.94mm^{-1} for the 2.85mm thick filter and experimental waveform is given in Fig. 6b and it can be noted that the agreement is good. Similar results were also obtained using the Fabry-Perot interferometer and are shown in Fig. 7. In this plot the signal is delayed, as the wave has to propagate through both the sample of thickness 1.63mm and the FP mirror of thickness 9mm before it is detected. It can be noted that the signal has qualitatively similar SNR characteristics.

The use of laser based detection scheme in OAI for noncontact, broadband detection of ultrasound directly off of the target surface is an exciting prospect. This should offer the ability to detect small objects buried in highly scattering media. A path stabilized Michelson interferometer was used to detect ultrasonic signals directly off of the acrylamide tissue-mimicking phantom described above. In this case sufficient light was reflected back to the interferometer from the polystyrene particles. The acoustic wave

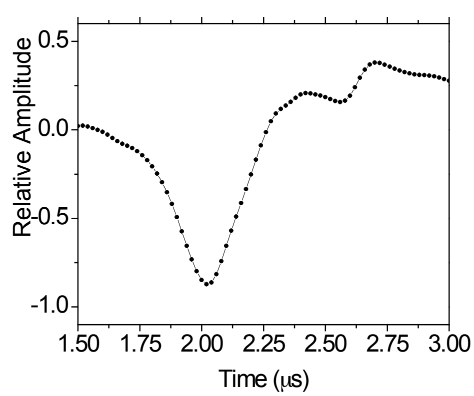

FIGURE 7. Forward mode displacement observed on a neutral density filter of thickness 1.63mm and 9mm thick FP mirror using the Fabry-Perot interferometer

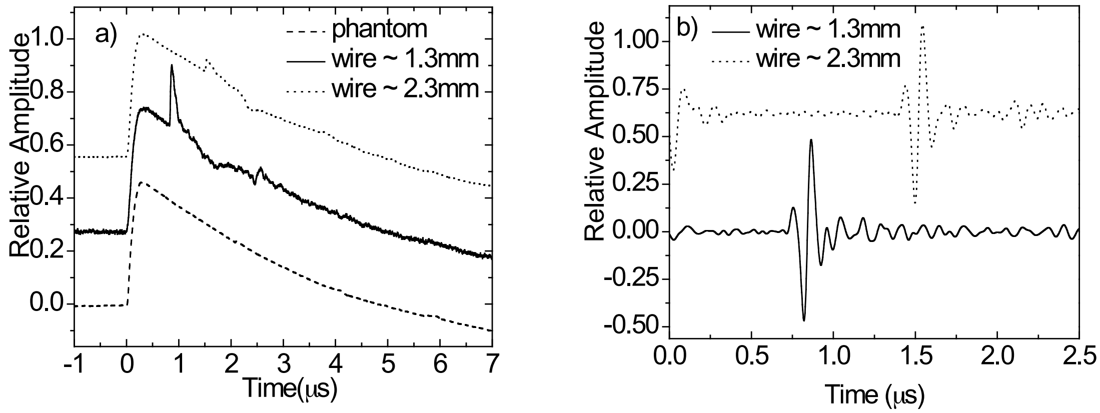

FIGURE 8. a) Signals obtained in the backward mode on the scattering phantom with a 400μm wire buried at different depths using path-stabilized michelson interferometer b) High pass filtered signals from the sample wire buried in the scattering phantom

speed and the density of the phantom were measured to be 1.52mm/μs and 1.05g/cc respectively. A wire of diameter 400μm was embedded in the phantom at distances of 1.3mm, and 2.3mm and the signals were obtained. These backward mode displacement plots are shown in Fig. 8a. ANSI standards set the safe level of laser irradiation of skin in the near infrared spectral range at 0.1-0.2 J/cm^2 [17] and the experiments were performed at approximately 0.01 J/cm^2, which is well within the range. The high frequency transient from the wire can be observed on the background signal. High pass filtered signals are shown in Fig. 8b which eliminates the background signal from homogeneous absorption of light within the sample and shows only the higher frequency signals generated by the optical inhomogeneity within the turbid media.

CONCLUSION

In this paper optical detection of optoacoustic transients is demonstrated. Optical detection of optoacoustic transients has several potential advantages over the use of contact transducers: optical systems are inherently broadband and can easily cover the useful frequency range for medical imaging, the optical source and receiver can be co-located on the specimen surface, and it is possible to fabricate optical array detectors using diffractive optics. Detection of optoacoustic signals in both homogeneous and inhomogeneous phantoms is demonstrated. It is shown that there is sufficient sensitivity for near surface imaging.

REFERENCES

1. Gusev, V.E. Karabutov, A.A., *Laser Optoacoustics*, AIP Press; NewYork, 1993.
2. Scruby, C. B. and Drain, L.E., *Laser-Ultrasonics: Techniques and Applications*, Adam Hilger, Bristol, UK, 1990.
3. Davis, A. Ohn, M. M. Liu, K. and Measures, R. M., 1991, A study of an opto-ultrasonic technique for cure monitoring *Proc. SPIE*, **1588** 264-74.
4. Oraevsky, A. A. and Karabutov, A. A., in *Handbook of Optical Biomedical Diagnostics* (V.V. Tuchin, editor) pp.585-646, SPIE press, WA (2002).
5. Oraevsky, A. A. Biomedical Optoacoustics II, Progress in Biomedical Optics and Imaging, *Proc. SPIE*, **4256** pp. 1-84, 147-166 (2001).

6. Paltauf, G. Schmidt-Kloiber, H. Kostli, K.P. and Frenz, M., *Appl. Phys. Lett.*, **75** (8), pp. 1048-1050, (1999).
7. Beard, P.C. and Mills, T.N., *Proc. SPIE*, **4256** pp. 34-42.
8. Hamilton, J.D. and O'Donnell, M. IEEE Trans. Ultra., Ferroelect., and Freq. Contr., **45** (1) pp. 216-235, (1998).
9. Hamilton, J. D. Buma, T. Spisar, M. and O'Donnell, M., *IEEE Transactions on ultrasonics, ferroelectrics, and frequency control*, **47** (1), pp. 160-169 (2000).
10. Rose, L.F.R., J Acoustic Soc. Am, **75** pp. 1613-1623, (1986).
11. Spicer, J. (1991). *Laser ultrasonics in finite structures: comprehensive modeling with supporting experiment*. Ph. D. thesis, The John Hopkins University.
12. Ing, R.K. and Monchalin, J.P., *Appl. Phys. Lett*., **59** (25), pp.3233-3235, (1991).
13. Murray, T. W. Tuovinen, H. and Krishnaswamy, S., *Appl. Optics*, **39** (19) pp.3276-3284, (2000).
14. Hurley, D.C. and Fortunko, C.M., *Meas. Sci. Technol.*, **8** pp. 634-642, (1997).
15. Viator, J. A. and Prahl, S. A., *Proc. SPIE*, **3601**, 276-283, (1999)
16. Telshow, K. L. and Conant, R. J., *J. Acoust. Soc. Am.*, **88** (3), 1990, p. 1494.
17. American National Standard for Safe Use of Lasers, ANSI Standard Z136.1, 1993.